ELSEVIER

Comput. Methods Appl. Mech. Engrg. 136 (1996) 27–46

Computer methods in applied mechanics and engineering

A Petrov–Galerkin formulation for advection–reaction–diffusion problems

S. Idelsohn[a,*], N. Nigro[a], M. Storti[a], G. Buscaglia[b]

[a]*Grupo de Tecnología Mecánica del INTEC, Universidad Nacional del Litoral and CONICET, Güemes 3450, 3000, Santa Fe, Argentina*

[b]*División Mecánica Computacional, Centro Atómico Bariloche e Instituto Balseiro, 8400 San Carlos de Bariloche, Argentina*

Received 10 March 1994; revised 9 July 1995

Abstract

In this work we present a new method called (SU + C)PG to solve advection–reaction–diffusion scalar equations by the Finite Element Method (FEM). The SUPG (for *Streamline Upwind Petrov–Galerkin*) method is currently one of the most popular methods for advection–diffusion problems due to its inherent consistency and efficiency in avoiding the spurious oscillations obtained from the plain Galerkin method when there are discontinuities in the solution. Following this ideas, Tezduyar and Park treated the more general advection–reaction–diffusion problem and they developed a stabilizing term for advection–reaction problems without significant diffusive boundary layers. In this work an SUPG extension for all situations is performed, covering the whole plane represented by the Peclet number and the dimensionless reaction number. The scheme is based on the extension of the super-convergence feature through the inclusion of an additional perturbation function and a corresponding proportionality constant. Both proportionality constants (that one corresponding to the standard perturbation function from SUPG, and the new one introduced here) are selected in order to verify the 'super-convergence' feature, i.e. exact nodal values are obtained for a restricted class of problems (uniform mesh, no source term, constant physical properties). It is also shown that the (SU + C)PG scheme verifies the Discrete Maximum Principle (DMP), that guarantees uniform convergence of the finite element solution. Moreover, it is shown that super-convergence is closely related to the DMP, motivating the interest in developing numerical schemes that extend the super-convergence feature to a broader class of problems.

1. Introduction

In this paper we focus on the numerical solution of the advective–reactive–diffusive equation using the finite element method. Here, diffusion, advection and reaction refer to those terms in the governing equation involving second, first and zero order derivatives of the unknown variable. This kind of equation represents a simplified model for several industrial processes, for example the simulation of electrophoresis separation phenomena and the operation of a great number of chemical reactors. In these processes both the concentration and temperature play the role of the unknown variable. Another interesting application is found in the simulation of fluid flow in a non-inertial frame. This phenomenon is represented by an advective–reactive–diffusive system where the inertial forces are included in the advection term, the Coriolis forces are included in the reaction term and finally the diffusive part is due to the viscous effects. The dimensionless Reynolds and Rossby numbers quantify the relative magnitude of these forces. Both limits for high Rossby and Reynolds numbers have a lot of numerical and physical difficulties, specially concerning with the stability of the fluid flow and the scheme used to simulate it.

* Corresponding author.

PPI 0045-7825(96)01008-0

One of the major goals of this paper is to solve the problem associated with the stabilization of the numerical scheme of an advective–reactive–diffusive system that arises from the simulation of fluid flow around turbomachines. Our main objective is to stabilize the numerical modelization of fluid flow around rotating stages of turbomachines, i.e. in non-inertial systems rotating with constant angular velocity. In this study we take the corresponding scalar equation as a first insight into the problem. Another interesting application of the results obtained in this paper is the numerical simulation of transient problems using semi-implicit or implicit methods. When the temporal term in a transient advective–diffusive equation is discretized, a term which is similar to the reaction one in an advective–reactive–diffusive equation is produced. For instance, solving the heat equation by an implicit temporal scheme with a very small time step produces numerical results that are vitiated with oscillations. These oscillations can be suppressed by limiting the minimum time step. But, in order to improve the accuracy of the results, it is very common to refine the mesh near local zones where the solution exhibits strong variations. With such an heterogeneous mesh we have to take the minimum time step to guarantee temporal accuracy in the refined zones but not so small in order to avoid the numerical oscillations. The strategy presented in this paper can be applied to overcome this intricate situation, stabilizing the scheme and allowing the use of the optimal mesh and time step to capture all the interesting features of the problem.

Now, let us take the steady, linear advective–diffusive equation. As it is well known, the numerical solution of the above equation using Galerkin formulations exhibits global spurious oscillations in advection dominated problems, specially in the vicinity of discontinuities. Such drawback can be overcome by the popular SUPG method [1]. This method stabilizes the numerical scheme by adding a perturbation to the weight function producing an oscillation free solution. This perturbation is proportional to the gradient of the standard interpolation function, so therefore for linear constant-size elements it is an odd function about the center node. The amount of perturbation to be incorporated is calculated as a function of the dimensionless Peclet number. By adding a shock capturing term one can preclude the overshoot and undershoot in the neighborhood of the discontinuities [2].

On the other hand, another kind of problem exists in reaction dominated problems associated with the existence of local oscillations, also near discontinuities, even in the absence of advection terms. Similarly to the advection dominated problems, Tezduyar and Park [3] added another perturbation to the weight function. They choose it to be proportional to the gradient of the standard weight function, like the perturbations used in advection dominated problems. The stabilization parameter is a constant. The importance of the reaction term can be quantified by a dimensionless number, which we call the *reaction number* r formed by the reaction constant, the advection velocity and the element length. This scheme, which is called DRD, is designed to give the nodally exact solution for the homogeneous, one-dimensional analysis when the reaction number is much greater than the others and there are no diffusive boundary layers. One of the most remarkable critics of the above scheme is that, when the advection and the reaction terms are important, it is very difficult to know what amount of each perturbation function should be added. Another important criticism stems from symmetry considerations under coordinate inversion $x \rightarrow -x$. In the reactive–diffusive case (null advection), the equation is invariant under this symmetry operation and it is clear that the weight function should be symmetric. Actually, this is not the case of this scheme.

In this direction this paper tries to give an answer to the above questions. We present a Petrov–Galerkin formulation proposing two different perturbations to the weight function, one of them is similar to that of SUPG scheme and the other one is symmetric. For advection–diffusion problems, the scheme is reduced to the standard SUPG scheme. On the other hand, for reaction–diffusion problems only the symmetric perturbation subsists and the scheme is called CPG from '*Centered Petrov–Galerkin*'. In intermediate situations the scheme is a combination of the two, and then the acronym (SU + C)PG. The proportionality constant for each perturbation depends on the two dimensionless numbers, Peclet number Pe and the reaction number r. We find two expressions $\alpha(\mathrm{Pe}, r)$, $\gamma(\mathrm{Pe}, r)$ similarly as with the magic function in SUPG, where α, γ are the proportionality constants for both perturbation terms. With this kind of solution, we can solve in an optimal way not only the limit cases $\mathrm{Pe} \rightarrow \pm\infty$, $r \rightarrow \infty$, but also the whole Pe-r plane.

Another alternative to solve the previous problem, introduced by Codina [4], consists in using an

SUPG formulation with shock capturing including the stabilization of the reactive effects in this last term. He demonstrated that the original equation can be transformed in a new advective–diffusive equation with a transformed velocity. Then, he applied the well-known schemes to this kind of problem.

Later, seeking the generalization of the great number of stabilization algorithms, a new strategy was developed to solve the problems associated with the existence of oscillations. It was called *Galerkin Least Squares* (GLS) and is based on a Galerkin formulation but using a least-squares form of the Euler–Lagrange equation. This method, introduced by Hughes [5], was applied to Stokes flow problems and incompressible elasticity problems. With this formulation it was possible to use equal order interpolation for pressure and velocity variables within a Galerkin context. Then, they extend these results to several mixed formulations and to the linear advective–diffusive systems [6]. In order to adapt the previous method to reactive dominated problems, Franca et al. [7] proposed the *Galerkin Gradient Least Squares* (GGLS) that uses a Galerkin formulation and a least squares form of the gradient of Euler–Lagrange in order to suppress the local oscillations due to the presence of reactive terms.

In Section 2, we find the one-dimensional stencil over an uniform mesh that gives a stable numerical scheme, getting the nodally exact solution. In Section 3 we transform this scheme to a Petrov–Galerkin formulation adding a new perturbation function to the standard SUPG weighing function and we show that the proportionality constants α and γ, affecting the perturbation terms, behave correctly in the limit cases, the advection-dominated and the reactive-dominated flow. In Section 4 the Discrete Maximum Principle is discussed, and the region of stability for the (SU + C)PG method is assessed, as well as for the Galerkin method, SUPG and DRD. In Section 5 an extension of the original scheme to the multidimensional case is presented. Finally, in Section 6 we present numerical results in two one-dimensional examples where we show the robustness of this method to several Pe and r conditions and including source terms and, finally, we present a multidimensional example.

2. Optimal numerical scheme for the one-dimensional problem

Let us consider the following simplified, one-dimensional form of the advection–reaction–diffusion equation:

$$\begin{aligned} &-k\phi'' + u\phi' + c\phi = f\,, \qquad 0 \leqslant x \leqslant 1\,, \\ &\phi(x=0) = \phi_0\,, \\ &\phi(x=1) = \phi_1\,, \end{aligned} \tag{1.1–3}$$

where $k > 0$ represents the physical diffusivity, u the transport velocity, ϕ the scalar unknown variable, $c \geqslant 0$ the reaction constant and f the source term. The weak formulation is

$$\int_\Omega (kw_i'\phi' + uw_i\phi' + cw_i\phi)\,\mathrm{d}\Omega + \sum_{e=1}^{N} \int_{\Omega_e} p_i(-k\phi'' + u\phi' + c\phi)\,\mathrm{d}\Omega = \int_\Omega \tilde{w}_i f\,\mathrm{d}\Omega\,, \quad i = 1, \ldots, N-1\,. \tag{2}$$

Where w_i are the standard linear trial functions, $\tilde{w}_i$ the weight functions:

$$\begin{aligned} &\tilde{w}_i = w_i + p_i\,, \\ &p_i = \alpha h w_i' + \gamma P_{2i}\,, \end{aligned} \tag{3}$$

p_i is the perturbation term and i, e are node and element indices, respectively. The first term is the well-known SUPG perturbation term, whereas the second one is the new perturbation function which is intended to stabilize the reactive effects. With different expressions for the proportionality constants α and γ we obtain the (SU + C)PG method as well as those ones found in the literature:

$$\begin{aligned} &\alpha = 0\,, && \gamma = 0\,, && \text{Galerkin}\,,\\ &\alpha = \coth \mathrm{Pe} - 1/\mathrm{Pe}\,, && \gamma = 0\,, && \text{SUPG}\,,\\ &\alpha = \alpha_{\mathrm{DRD}}(r/4\mathrm{Pe})\,, && \gamma = 0\,, && \text{DRD}\,,\\ &\alpha = \alpha_{(\mathrm{SU+C})\mathrm{PG}}(\mathrm{Pe}, r)\,, && \gamma = \gamma_{(\mathrm{SU+C})\mathrm{PG}}(\mathrm{Pe}, r)\,, && (\mathrm{SU}+\mathrm{C})\mathrm{PG}\,, \end{aligned} \tag{4.1–4}$$

where α_{DRD} is given by

$$\alpha_{\mathrm{DRD}}(x) = \tfrac{1}{2}\{-\coth(x) + x[1/\sinh(x)^2 + 4/6]\}/[1 - x\coth(x)]\,. \tag{5}$$

The dimensionless parameters Pe and r, quantifying advection and reaction, respectively, with respect to the diffusive term are defined as

$$\mathrm{Pe} = \frac{uh}{2k}\,, \qquad r = \frac{ch^2}{k}\,. \tag{6}$$

The expressions for $\alpha_{(\mathrm{SU+C})\mathrm{PG}}(\mathrm{Pe}, r)$ and $\gamma_{(\mathrm{SU+C})\mathrm{PG}}(\mathrm{Pe}, r)$ for the (SU + C)PG method in this work will be presented later.

Then, for a uniform h size mesh and for constant physical properties the computation of element contributions over each node produces the following difference equation:

$$\frac{(k+k^*)}{h^2}(-\phi_{i+1} + 2\phi_i - \phi_{i-1}) + \frac{(u+u^*)}{2h}(\phi_{i+1} - \phi_{i-1}) + \frac{(c+c^*)}{6}(\phi_{i+1} + 4\phi_i + \phi_{i-1}) = \tilde{f}_i\,. \tag{7}$$

The asterisk indicates those terms which come from the perturbation term, and which will be defined later. The right-hand side term is $\tilde{f}_i = \int_\Omega \tilde{w}_i f\, \mathrm{d}\Omega$. Its explicit expression in terms of $\{\tilde{f}_j\}_{j=i-1,i+1}$ is irrelevant to the study of the stability of the method. The case $p_i \equiv 0$, and consequently k^*, u^*, $c^* = 0$, corresponds to the Galerkin, non-stabilized, scheme. As it is well known, this formulation exhibits global spurious oscillations in the advection dominated case and also local oscillations when reaction dominates. We will design a perturbation function in such a way as to stabilize the scheme in the general case. To do that, we will follow a two-step procedure. Firstly, we will solve the appropriate discrete problem, i.e. to find the *numerical* k^*, u^* and c^* parameters, as function of mesh size and the physical constants k, u and c. Secondly, we design the perturbation function and proportionality constants to produce the desired stencil.

As it is usual in the SUPG context, these numerical parameters are found by requiring that the exact fundamental solutions to (1) in the homogeneous ($f \equiv 0$) case must be solutions of the discrete counterpart. The exact solutions are of the form:

$$\phi(x) = a\,\mathrm{e}^{\lambda_1 x} + b\,\mathrm{e}^{\lambda_2 x}\,, \tag{8}$$

where

$$\lambda_{1,2} = \frac{u}{2k} \pm \sqrt{\left(\frac{u}{2k}\right)^2 + \frac{c}{k}}\,, \tag{9}$$

and a, b are constants to be determined from the boundary conditions. Replacing (8) in (7), a system of two equations in k^*, u^* and c^* is obtained. In order to have a determined system we drop the c^* term. In fact, it can be shown that a different choice for $c^* = 0$, will lead to a stencil which is proportional to the original one. The expressions for k^* and u^* are

$$k + k^* = -ch^2\,\frac{2 + \mathrm{e}^{\lambda_1 h} + \mathrm{e}^{\lambda_2 h} + 2\,\mathrm{e}^{(\lambda_1+\lambda_2)h}}{6(1 - \mathrm{e}^{\lambda_1 h})(1 - \mathrm{e}^{\lambda_2 h})}\,, \tag{10.1}$$

$$u + u^* = ch\,\frac{1 - \mathrm{e}^{(\lambda_1+\lambda_2)h}}{(1 - \mathrm{e}^{\lambda_1 h})(1 - \mathrm{e}^{\lambda_2 h})}\,. \tag{10.2}$$

At first sight, the right-hand side of the expressions seem to vanish for $h \to 0$ due to the h^2 and h factors. This seems to be inconsistent (since it would imply $k^* \to -k$ for $h \to 0$), but note that both factors in the denominator also vanish, and the analysis is more involved. It will be shown later, in Section 3.2, that the scheme is consistent and, when the reaction is negligible, it tends to the known artificial diffusivity introduced by SUPG [1].

3. The (SU + C)PG method

In this section we design the second perturbation function P_2, and the proportionality constant $\alpha_{(SU+C)PG}$, $\gamma_{(SU+C)PG}$ in order to obtain the stencil given by Eqs. (7) and (10).

3.1. Second perturbation function

Since in the limit case of pure reaction the optimal weight function would be a Dirac's delta, it is reasonable to assume that $w + P_{2,i}$ must be of the form shown in Fig. 1. It is symmetric about the center node i and vanishes at the neighboring nodes $i \pm 1$. After straightforward integration of the elementary terms we arrive to the following stencil:

$$\frac{k + uah + k\gamma P_2(0)}{h}(-\phi_{i+1} + 2\phi_i - \phi_{i-1}) + \left(\frac{u - \alpha ch}{2} + u\gamma a\right)(\phi_{i+1} - \phi_{i-1})$$
$$+ \frac{ch}{6}(\phi_{i+1} + 4\phi_i + \phi_{i-1}) + c\gamma hm(\phi_{i+1} - 2\phi_i + \phi_{i-1}) + c\gamma ha2\phi_i = (\text{rhs})_i \,, \tag{11}$$

which depends only on three geometrical parameters of P_2, namely: the value at the center node $P_2(0)$, the dimensionless semi-area a and the dimensionless first moment of one-half of the function m:

$$ha = \int_{x_i}^{x_{i+1}} P_2(x)\,\mathrm{d}x \,,$$
$$h^2 m = \int_{x_i}^{x_{i+1}} (x - x_i) P_2(x)\,\mathrm{d}x \,. \tag{12}$$

Rearranging the above stencil (11) we arrive at a 2×2 system in α and γ:

$$\begin{bmatrix} g_{11} & g_{12} \\ g_{21} & g_{22} \end{bmatrix} \begin{bmatrix} \alpha_{(SU+C)PG} \\ \gamma_{(SU+C)PG} \end{bmatrix} = \begin{bmatrix} f_1 \\ f_2 \end{bmatrix} , \tag{13}$$

where

$$g_{j1} = [4\,\mathrm{Pe}(1 - \cosh(\lambda_j h) - r\sinh(\lambda_j h)] \,,$$
$$g_{j2} = 2[\cosh(\lambda_j h)(rm - P_2(0) + 2\,\mathrm{Pe}\,a\sinh(\lambda_j h + (P_2(0) - mr + ar)] \,, \tag{14}$$

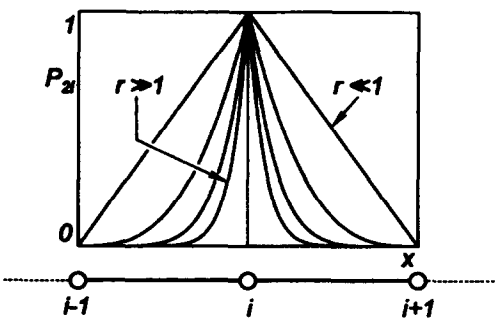

Fig. 1. Ideal weight functions for the null advection case.

$$f_j = -2[\cosh(\lambda_j h)(r/6 - 1) + \mathrm{Pe}\sinh(\lambda_j h) + (1 + r/3)]\,,$$

$$\lambda_j h = \mathrm{Pe} + (-1)^{j-1}\sqrt{\mathrm{Pe}^2 + r}\,,$$

for $j = 1, 2$.

We can obtain a super-convergent scheme by choosing an arbitrary function P_2 and computing α and γ from the preceding expression. However, for an arbitrary choice we will find, in general, that the proportionality constants have singularities for certain values of Pe and r, so that a design of the P_2 function is needed to avoid singularities. First, we recall that the previous expressions for α and γ only involve 3 geometrical parameters of the perturbation function P_2. A detailed study [8] shows that there are no singularities if $P_2(0) = 0$ and P_2 is negative definite. The lowest order polynomial (inside each element) that fulfills this requirements is (see Fig. 2):

$$P_2(\xi) = -\frac{1}{4}(1 - \xi^2)\,, \tag{15}$$

where ξ is the coordinate in the master element $|\xi| \leq 1$. The geometrical parameters corresponding to this function are: $P_2(0) = 0$, $a = -1/6$ and $m = -1/12$.

3.2. The proportionality constants

We refer to (SU + C)PG as the Petrov–Galerkin method based on the variational formulation (2), with the perturbation function defined by (3) and (15), and the proportionality constants defined by (14). In some limits the expressions are undeterminated, as it is also the case for the *magic function* of SUPG (see Eq. (4.2)), but this singularities are removable. In Figs. 3–6 we show them, and we see that they are bounded and well-behaved: $0 \leq \alpha \leq (1/2)$ and $0 \leq \gamma \leq 2$ for all Pe, r.

Regarding consistency, it can be shown that the proportionality constants can be approximated, for small Pe and r by

$$\alpha \sim \frac{\mathrm{Pe}}{6}\left(1 - \tfrac{2}{15}r\right)$$

$$\gamma \sim \frac{r}{4}\left(1 - \frac{r}{60}\right) \tag{16}$$

and $\mathrm{Pe} \sim h$ and $r \sim h^2$ for $h \to 0$. Then, it can be shown that all of the *numerical additives* k^*, u^* and c^*, which can be deduced from (7) and (11) vanish like $\sim h^2$ with mesh refinement.

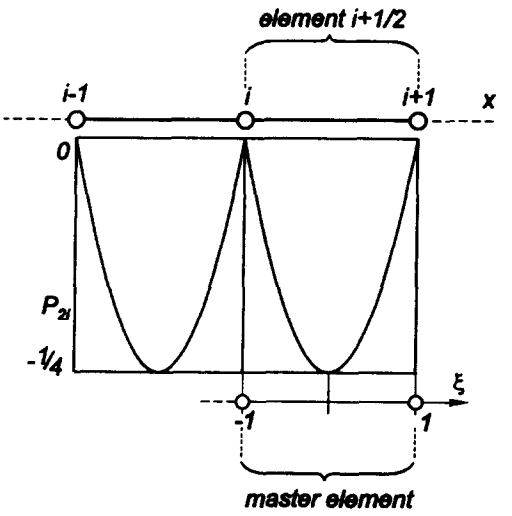

Fig. 2. Proposed second perturbation function P_2.

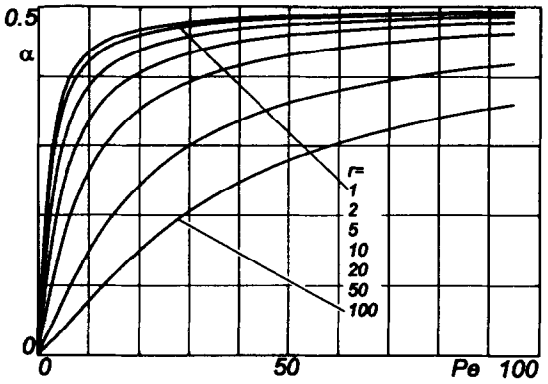

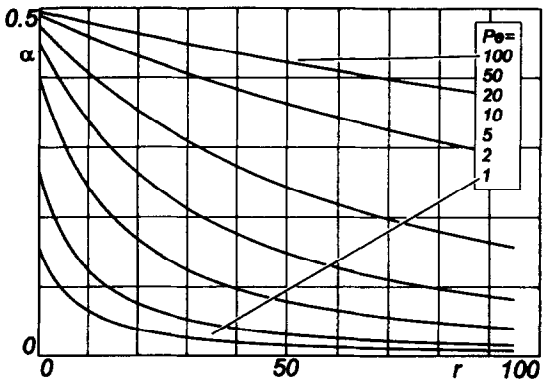

Fig. 3. Proportionality constant for the standard SUPG perturbation term α as function of Pe for constant r.

Fig. 4. Proportionality constant for the standard SUPG perturbation term α as function of r for constant Pe.

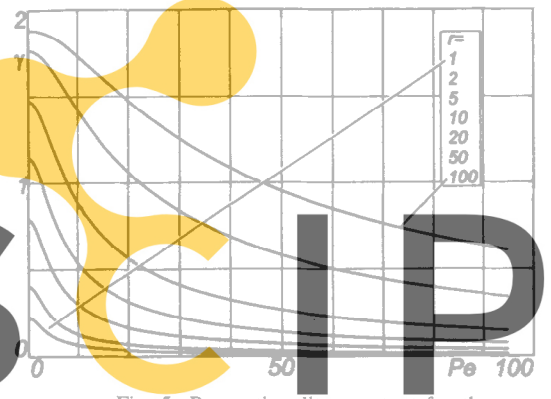

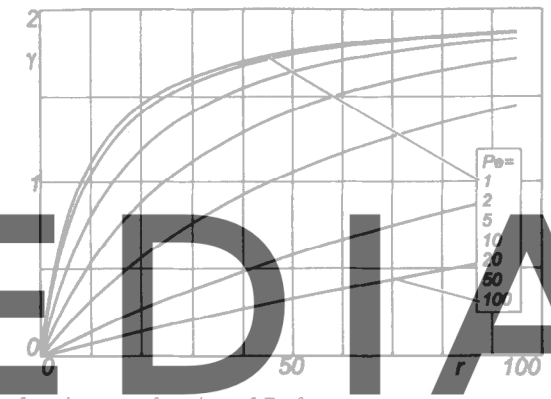

Fig. 5. Proportionality constant for the second perturbation function γ as function of Pe for constant r.

Fig. 6. Proportionality constant for the second perturbation function γ as function of r for constant Pe.

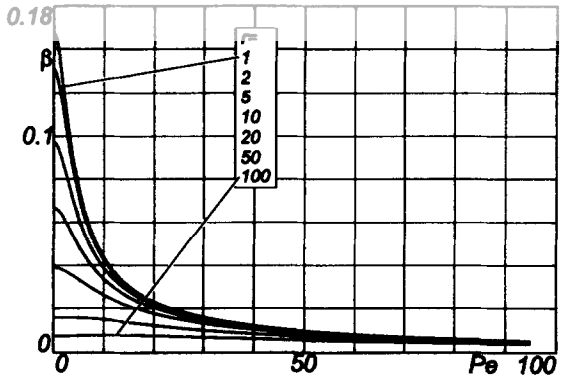

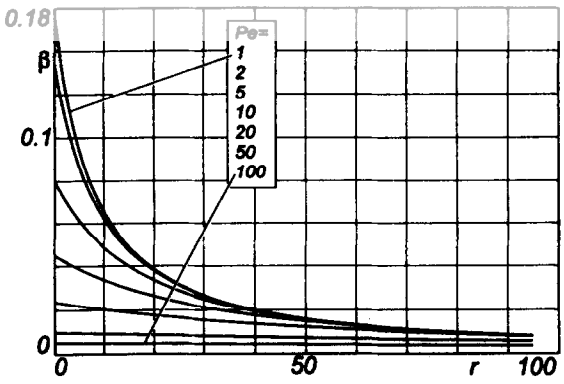

Fig. 7. Related proportionality constant for the second perturbation function β as function of Pe for constant r.

Fig. 8. Related proportionality constant for the second perturbation function β as function of r for constant Pe.

Moreover, some desirable limits are automatically satisfied. For instance, we recover SUPG with the standard magic function in the case of null reaction:

$$\left.\begin{aligned}\alpha &= \frac{1}{2}\,\mathrm{sign}(u)\left(\coth \mathrm{Pe} - \frac{1}{\mathrm{Pe}}\right)\\ \gamma &= 0\end{aligned}\right\} \quad \text{for } r = 0\,. \tag{17}$$

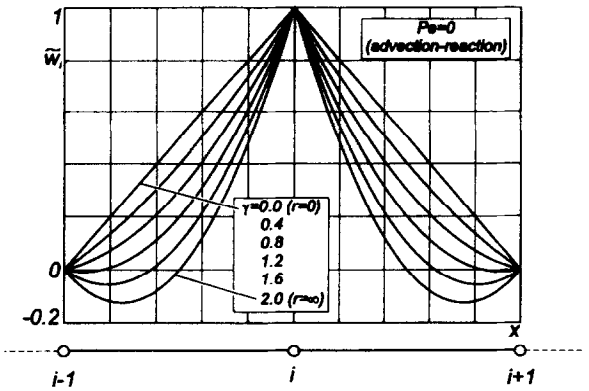

Fig. 9. Weight functions for the null advection case.

On the other hand, for null advection:

$$\left.\begin{aligned}\alpha &= 0\\ \gamma &= 12\,\frac{\cosh(\sqrt{r})(r/6-1)+(1+r/3)}{r[1+\cosh(\sqrt{r})]}\end{aligned}\right\} \quad \text{for Pe} = 0\,. \tag{18}$$

It takes the value $\gamma = 2$ as $r \to \infty$ and $\gamma = 0$ at $r = 0$. Relations (17, 18) can be observed as limit cases in Figs. 3–6. The whole family of weight functions for null advection is shown in Fig. 9 from $\gamma = 0$ to 2. The weight function concentrates in the center node as γ increases. For $\gamma = 2$ (pure reaction) the weight function takes negative values near the neighboring nodes and it can be checked that the resulting discrete scheme is simply collocation.

With respect to the computational cost involved in the calculation of the proportionality constants, it amounts to the evaluation of 4 exponentials, 2 square roots and 49 operations (additions, multiplications and divisions). For reference, the DRD method (expressions (4.3) and (5)) involves 3 functions and 15 operations, so that the cost of (SU + C)PG, is, at the most, 3 times higher than that of DRD. However, we will show, theoretically (Section 4) and through examples (Section 6), that the robustness and accuracy of (SU + C)PG largely pays this extra computational cost. On the other hand, the cost of those methods that resort to non-linear feedback of the solution, like the discontinuity-capturing techniques presented in [3] or [4], depends on the precision with which the non-linear problem is solved, but we can estimate that the cost of (SU + C)PG is well below them.

4. Theoretical assessment of the performance of (SU + C)PG

4.1. The DRD method

Under certain conditions, we can show that one of the terms in (8) can be neglected and then, the conditions on the numerical scheme can be relaxed by imposing that only the other exponential should be an exact solution of the numerical scheme. As only one equation is imposed on the numerical stencil, we can drop one of the perturbation functions, and we arrive to a scheme with only one perturbation function that exhibits *super-convergence* in those cases where the above assumptions are valid. This is the basis of the *DRD* method from Tezduyar and Park [3], who retained the usual perturbation function from SUPG and redefined the proportionality constant in order to match the relevant exponential term.

Consider the case of a one-dimensional problem as in (1) with fluid flowing from right to left ($u < 0$) constant physical properties, no source-term and Dirichlet boundary conditions $\phi_0 = 0$, $\phi_1 = 1$. The solution is given by

$$\phi = \frac{e^{\lambda_1 x} - e^{\lambda_2 x}}{e^{\lambda_1} - e^{\lambda_2}} = \phi_1 - \phi_2 \,. \tag{19}$$

But, as $u < 0$, we have $\lambda_1 > 0$, $\lambda_2 < 0$. The term ϕ_2 involving λ_2 decreases monotonically (in absolute value) so that the maximum value is attained at $x = 0$ and is

$$\max_x |\phi_2(x)| = |\phi_2(0)| = \frac{1}{e^{\lambda_1} - e^{\lambda_2}} \,. \tag{20}$$

Now, we assume that $|\mathrm{Pe}_L| \gg 1$ and $\mathrm{Pe}_L \ll r_L \ll \mathrm{Pe}_L^2$, where $\mathrm{Pe}_L = uL/2k$ and $r_L = cL^2/k$ are the non-dimensional numbers based on the length of the interval $L = 1$. The characteristic roots can be approximated as

$$\begin{aligned} \lambda_1 L &= \mathrm{Pe}_L + \sqrt{\mathrm{Pe}_L^2 + r_L} \approx r_L / |\mathrm{Pe}_L| \,, \\ \lambda_2 L &= \mathrm{Pe}_L - \sqrt{\mathrm{Pe}_L^2 + r_L} \approx 2\,\mathrm{Pe}_L \,. \end{aligned} \tag{21}$$

and then

$$e^{\lambda_1} \gg 1 \,, \qquad e^{\lambda_2} \ll 1 \,, \tag{22}$$

so that

$$|\phi_2(0)| \ll 1 \,, \tag{23}$$

and the solution (19) can be approximated as

$$\phi \approx \phi_1 = \frac{e^{\lambda_1 x}}{e^{\lambda_1} - e^{\lambda_2}} \approx e^{-c(1-x)/|u|} \,. \tag{24}$$

The DRD method is based on choosing the weighting function as

$$\tilde{w}_i = w_i + \alpha h w_{i,x} \,, \tag{25}$$

and choosing α in order to solve exactly for the term $e^{cx/u}$. The resulting expression is $\alpha = \alpha_{\mathrm{DRD}}$ (for 1D, as in (4)).

Note that approximation (24) can be obtained if the diffusive term in (1.1) is neglected and the resulting first order ODE is integrated from right to left taking (1.3) as the initial condition. This is the *inviscid solution*, since it does not depend on the magnitude of the diffusivity constant k (see Fig. 10). At the downwind boundary, the inviscid solution takes a value which is different, in general, from that

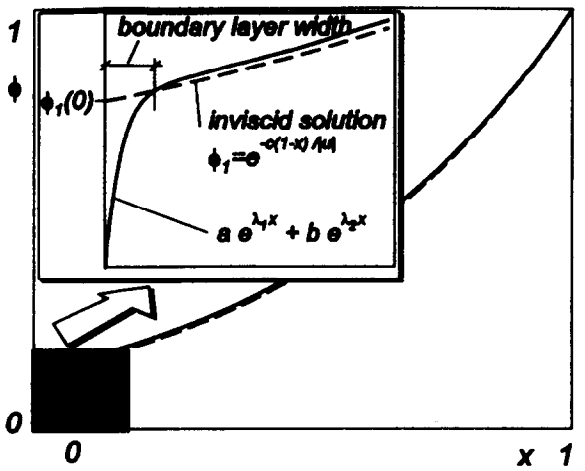

Fig. 10. High Pe and r case with downwind essential boundary condition.

one imposed by the boundary condition. This mismatch is absorbed in a sharp boundary layer whose width is roughly proportional to the diffusivity. Whenever the mismatch between the inner inviscid solution and the boundary value is small, the effect of the boundary layer can be neglected and the DRD algorithm will work. In the case of Eq. (1), the inviscid solution given by (24) takes the value $e^{-cL/|a|} = e^{-r_L/|\mathrm{Pe}_L|} \ll 1$ at the downwind boundary $x = 0$, so that the mismatch is small. This will also happen if the null flux condition $(\partial\phi/\partial x) = 0$ were imposed at $x = 0$. But it may also happen that if the inviscid solution is smooth enough, not only does the DRD work but Galerkin and SUPG will do as well. On the other hand, a large mismatch will be produced if the boundary value in (1.2) is different from zero, or if $r_L/|\mathrm{Pe}_L|$ is not so large, as in case A_3 to be discussed later in the numerical results. In these cases it is expected that the DRD method does not work properly.

4.2. The Discrete Maximum Principle

Now, we will show that the (SU + C)PG scheme verifies the *Discrete Maximum Principle* (DMP), for all Pe and r, whereas the others (Galerkin, SUPG and DRD) only satisfy the DMP in restricted regions of the Pe-r plane. We will call these regions the *stability regions* of each method.

It is well known that the continuum problem satisfies a maximum principle, which can be put in the following terms: if $f(x) \leq 0$ for all x, then ϕ attains its maximum at the boundaries. The question is whether the discrete scheme inherits this feature, i.e. if, for any $f(x) \leq 0$ the numerical solution satisfies: $\phi_i \leq \max\{\bar{\phi}\}$ for all i, where $\bar{\phi}$ is the value of ϕ at the boundaries. It has been shown [9] that the satisfaction of the DMP implies uniform convergence of the finite element solution. A sufficient condition to check the validity of the DMP is to verify the following conditions on the coefficients of the discrete matrix $\boldsymbol{K}$, representing the numerical discretization of the differential operator presented in (1.1–8):

$$\begin{aligned} &K_{ij} < 0\,, \quad \text{for } i \neq j\,, \\ &\sum_j K_{ij} \geq 0\,, \quad \text{for all } i\,. \end{aligned} \tag{26}$$

For the instance of a uniform mesh, the elements of the matrix $\boldsymbol{K}$ are

$$\boldsymbol{K}_{ij} = \begin{cases} c_{-1}\,; & \text{if } j = i-1\,, \\ c_0\,; & \text{if } j = i\,, \\ c_1\,; & \text{if } j = i+1\,, \\ 0\,; & \text{otherwise}\,, \end{cases} \tag{27}$$

and so, the conditions (26) can be written as

$$\begin{aligned} &c_{-1}, c_1 < 0\,, \\ &c_{-1} + c_0 + c_1 > 0\,. \end{aligned} \tag{28.1, 2}$$

On the other hand, the coefficients c_i can be transformed into a dimensionless form: $c_i = k/h\tilde{c}_i(\mathrm{Pe}, r)$, so that (28) define the stability regions for each method.

4.3. The DMP for the Galerkin, SUPG and DRD methods

The non-dimensional coefficients can be easily obtained from (11):

$$\begin{aligned} \tilde{c}_{\pm 1} &= -1 \mp \mathrm{Pe} + \tfrac{1}{6}r - 2\alpha\,\mathrm{Pe} \pm \tfrac{1}{2}\alpha r\,, \\ \tilde{c}_0 &= 2 + \tfrac{2}{3}r + 4\alpha\,\mathrm{Pe}\,, \end{aligned} \tag{29}$$

where α is defined for each case as in (4). Condition (28.2) is always satisfied, since $c_{-1} + c_0 + c_1 = r$. Then, the regions of stability arised from condition (28.1) are (see Fig. 11):

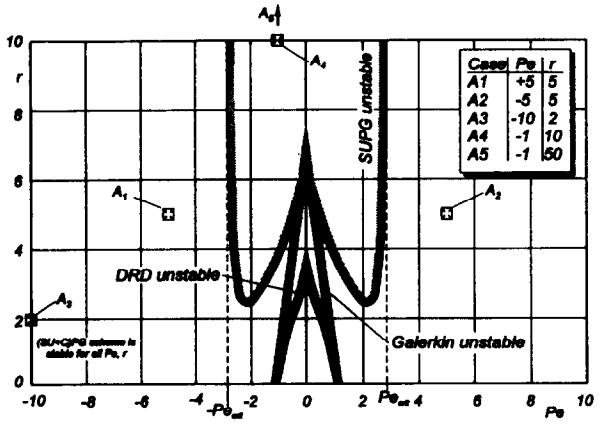

Fig. 11. Stability map for Galerkin, DRD and SUPG.

$$
\begin{aligned}
&r < 6(1 + |\mathrm{Pe}|)\,, \quad \text{for Galerkin}\,,\\
&r < \begin{cases} 6(1 - |\mathrm{Pe}| + 2\alpha\,\mathrm{Pe})/(1 - 3|\alpha|)\,, & |\mathrm{Pe}| < \mathrm{Pe}_{\mathrm{crit}}\,;\\ \infty\,, & |\mathrm{Pe}| > \mathrm{Pe}_{\mathrm{crit}}\,; \end{cases} \quad \text{for SUPG}\,,\\
&r < 4|\mathrm{Pe}|g(|\mathrm{Pe}|)\,, \quad \text{for DRD}\,,
\end{aligned}
\tag{30}
$$

where $\mathrm{Pe}_{\mathrm{crit}} \approx 2.9515$ is the solution of $\frac{1}{2}[\coth(\mathrm{Pe}_{\mathrm{crit}}) - 1/\mathrm{Pe}_{\mathrm{crit}}] = \frac{1}{3}$, and g is defined implicitly by

$$1/x = -1 + \tfrac{2}{3}g(x) + 2[g(x) - 1]\alpha_{\mathrm{DRD}}(g(x))\,. \tag{31}$$

The region of stability for Galerkin is a triangle, for pure advection the range of admissible Peclets is $|\mathrm{Pe}| < 1$, where for pure reaction we must have $r < 6$. SUPG has a much broader range of stability. Needless to say, for pure advection all the Pe axis is in the stable zone, and for $|\mathrm{Pe}| > \mathrm{Pe}_{\mathrm{crit}}$ it is stable for all r. However, for pure reaction the range of stable reaction numbers is the same as Galerkin ($r < 6$).

On the other hand, the DRD method has a stable region smaller than Galerkin's. However, as it was discussed previously, the interest of DRD is only for some particular cases, roughly speaking, those ones with natural downwind boundary conditions.

4.4. The DMP for the (SU + C)PG scheme

As the (SU + C)PG discrete scheme exhibits super-convergence, then the general solution of the discrete system with no source term should coincide with the discrete values of (8). So that:

$$c_1\rho_i^2 + c_0\rho_i + c_{-1} = 0\,, \tag{32}$$

where

$$\rho_i = \mathrm{e}^{\lambda_i h}\,. \tag{33}$$

This gives two equations relating the values of c_1, c_0 and c_{-1}, so that we can eliminate c_1 and c_{-1} in terms of c_0:

$$c_1 = -c_0/(\rho_1 + \rho_2)\,, \qquad c_{-1} = -c_0\rho_1\rho_2/(\rho_1 + \rho_2)\,. \tag{34}$$

It is clear from (9) that both eigenvalues are real and $\lambda_1 > 0$, $\lambda_2 < 0$ for $u > 0$. This implies that the ρ_i are also real and positive, and $\rho_1 > 1$, $\rho_2 < 1$. Then, (34) shows that c_1 and c_{-1} have opposite sign respect to c_0. But, from (11):

$$c_0 = k/h[1 + 2\,\mathrm{Pe}\,\alpha + \tfrac{1}{12}r(4 - \gamma)] > 0\,, \tag{35}$$

since Pe $\alpha \geq 0$ and $\gamma < 2$ for all Pe and r. Moreover:

$$c_1 + c_0 + c_{-1} = c_0 \frac{(\rho_1 - 1)(1 - \rho_2)}{\rho_1 + \rho_2} > 0 . \tag{36}$$

Note that this demonstration is rather independent of the particular scheme and can be extended easily to other kind of problems (system of equations, higher-order schemes, for instance), *whenever the scheme is based on the adjustment of the numerical coefficients in order to match the solutions for the homogeneous case.*

5. Extension to the multidimensional case

The weight function has the same expression as in (3) with the only modification that, now, α is a vector. We will explain how this extension is achieved in 2D. The extension to the 3D case is straightforward. P_2 is taken as the cartesian product of the corresponding 1D counterparts (see Fig. 12):

$$P_2(\xi, \eta) = -(1/16)(1 - \xi^2)(1 - \eta^2) . \tag{37}$$

where $|\xi|, |\eta| \leq 1$ are coordinates in the master element. It is remarkable that this is the same *bubble* function that stabilizes some pair of interpolation spaces in the mixed formulation of the Navier–Stokes equations. However, note that, here, this function is added only to the weight function, not to the space of interpolation functions.

An element size has to be chosen for the computation of α and ϕ. We have taken the corresponding value along the streamline:

$$h_s = 2\left(\sum_{i=1}^{N_{el}} |\hat{s} \cdot \nabla w_i| \right)^{-1} , \tag{38}$$

where $i = 1, \ldots, N_{el}$ are the nodes of the actual element. Streamline values Pe_s, r_s are computed and the corresponding α and γ parameters are reckoned. To extend α as a vector, we note, first, that the 1D SUPG perturbation term can be rewritten as:

$$\alpha(\mathrm{Pe}, r) h w' = \beta \frac{uh^2}{2k} w' , \quad \text{with} \quad \beta(\mathrm{Pe}, r) = \frac{\alpha(\mathrm{Pe}, r)}{\mathrm{Pe}} . \tag{39}$$

It can be seen from Fig. 3 that $\alpha = \mathrm{O}(\mathrm{Pe})$ for $\mathrm{Pe} \to 0$ and $r =$ constant, so the quotient $\beta = \alpha / \mathrm{Pe}$ is well behaved (see Figs. 7–8) and, then, the corresponding extension to the multidimensional case is:

$$\beta(\mathrm{Pe}_s, r_s) \frac{h_s^2}{2k} (\boldsymbol{u} \cdot \nabla w) . \tag{40}$$

In order to improve the performance of the present scheme, a shock capturing term can be added,

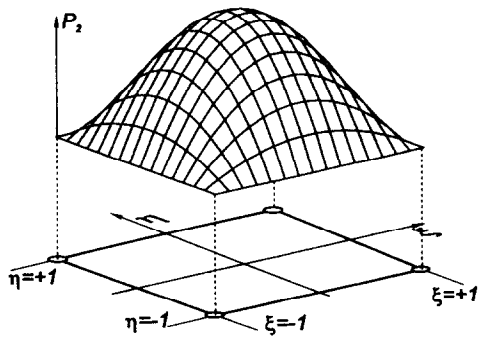

Fig. 12. 2D extension of the perturbation function P_2.

reducing overshoot and undershoot effects in the vicinity of discontinuities. To perform this task we select an element size in the direction of the solution gradient and we compute the respective proportionality constants $\beta_{\|}$, $\gamma_{\|}$. The $\beta_{\|}$ term is treated in the same way as it is usual in the SUPG context [2]. As regards $\gamma_{\|}$, it straightforwardly replaces γ in the perturbation function.

6. Numerical results

6.1. Generation of non-uniform meshes

As the scheme is super-convergent, the interesting examples are those where at least one of the conditions for super-convergence are violated. In order to generate non-uniform meshes, the coordinates of the nodal points are chosen according to

$$x_j = \begin{cases} 0\,; & j=0\,; \\ (j+\frac{1}{2}\delta_j)\bar{h}\,; & 1 \leqslant j \leqslant N-1\,; \\ 1\,; & j=N\,; \end{cases} \tag{41}$$

where $\bar{h}=1/N$ and the δ_j are randomly generated with a uniform distribution in the interval $0 \leqslant \delta_j \leqslant \delta_{\max}$, with $\delta_{\max} < 1$. In this way, an *ensemble* of meshes $\mathcal{M}$ is constructed with the following properties:

(1) All the meshes have N elements.
(2) The double averaged size of the elements $\langle \langle h_e \rangle_{e \in M} \rangle_{M \in \mathcal{M}}$ is $\bar{h}$.
(3) The maximum and minimum size of the elements are bounded by $h_{\max} \leqslant \bar{h}(1+\delta_{\max})$, $h_{\min} \geqslant \bar{h}(1-\delta_{\max})$.
(4) The maximum ratio of element sizes as in a given mesh is

$$\frac{h_{\max}}{h_{\min}} \leqslant \frac{1+\delta_{\max}}{1-\delta_{\max}}\,. \tag{42}$$

Of course, uniform meshes are generated for $\delta_{\max}=0$.

6.2. Experimental regions of stability. Comparison with other methods

To experimentally confirm the stability regions deduced previously, we performed a large number of numerical experiments simulating the problem described by (1) with no source term, and $\phi_0=0$, $\phi_1=1$. The region $|\mathrm{Pe}| \leqslant 10$, $0 \leqslant r \leqslant 10$ was covered with a grid of 100×50 points of the form $(\pm \mathrm{Pe}_j, r_l)$ where the Pe_j and r_l, $j, l = 1, \ldots, 50$ are interpolated logarithmically between 0.2 and 10. The mesh was non-uniform, generated as described in the previous section with 20 elements ($\bar{h}=\frac{1}{20}=0.05$) and $\delta_{\max}=0.95$. The physical properties k, u and c were set according to the values of Peclet and reaction numbers, considered as based on the average size element $\bar{h}$. Since the exact solution, given by (19), is monotone we used this as the criterion for stability, i.e. the discrete solution $\{\phi_i\}$ for a given set of parameters (Pe_j, r_l) is unstable if $\phi_{i+1} < \phi_i$ for some i.

The resulting *stability map* is shown in Fig. 13. It can be seen that the right portion of the map ($\mathrm{Pe} > 0$) is similar to the stability map based on the DMP (see Fig. 11). The differences can be attributed to the fact that the non-dimensional mesh parameters Pe and r are based in an average element size. In contrast, the left portion is qualitatively different from the DMP version. For all methods, the stability region for $\mathrm{Pe} < 0$ is much broader than that for $\mathrm{Pe} > 0$. This is because for a large part of the region $\mathrm{Pe} < 0$, the solution is rather smooth, even if $|\mathrm{Pe}|$ and r are large. For instance, consider the cases $\mathrm{Pe} = \pm 5$, $r = 5$ ($u = \pm 200$, $c = 2 \times 10^3$, as $\bar{h} = \frac{1}{20}$), indicated as A_1 and A_2 in Fig. 13. (The physical parameters are summarized in Table 1.) The corresponding profiles can be seen in Figs. 14 ($\mathrm{Pe} = +5$) and 15 ($\mathrm{Pe} = -5$). The solution for $\mathrm{Pe} < 0$ is rather smooth, since it is basically equal to the inviscid solution, which has a characteristic length of $\delta \approx |u|/c = \frac{1}{10}$ as explained in Section 4.1 and practically all methods give a qualitatively good result, even Galerkin. Actually, the DRD and SUPG

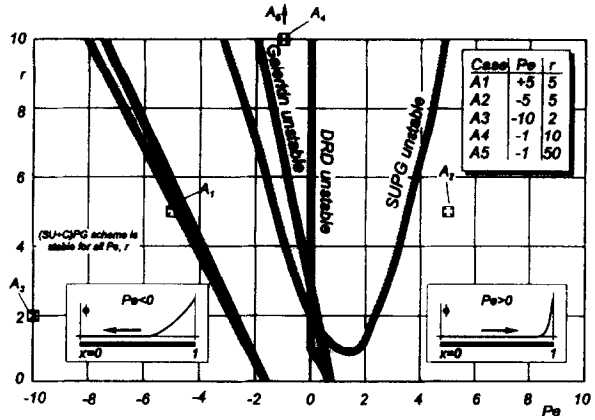

Fig. 13. Experimentally determined stability map for Galerkin, DRD and SUPG.

Table 1

Case	Fig.	Pe	r	u	c
A_1	14	+5	5	200	2000
A_2	15	−5	5	−200	2000
A_3	16	−10	2	−400	800
A_4	17	−1	10	−40	4000
A_5	18	−1	50	−40	20 000

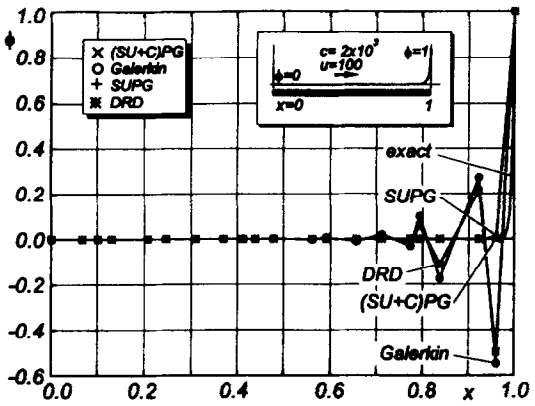

Fig. 14. One-dimensional example with non-uniform mesh. Case A_1.

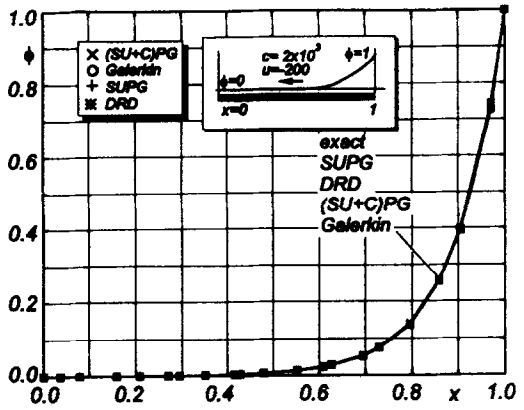

Fig. 15. One-dimensional example with non-uniform mesh. Case A_2.

method have a very small oscillation $\min_i\{\phi_{i+1} - \phi_i\} = O(10^{-6})$, produced by the boundary layer at the left boundary. Note that the position in the Pe-r plane is slightly inside the region of instability for both methods. In contrast, the solution for $u > 0$ exhibits a thin diffusive layer, with a characteristic length $\delta \approx k/|u| = \frac{1}{200}$, and only the SUPG and (SU + C)PG methods, which can cope with the strong diffusive boundary layer, give non-oscillatory results. Coming back to the $\mathrm{Pe} < 0$ case, if we move deeper into the instability region of both the DRD and Galerkin methods, as for case A_3 ($\mathrm{Pe} = -10$, $r = 2$, $u = -400$, $c = 800$, see Fig. 16), then the amplitude of the mismatch at the left boundary is larger, and both DRD and Galerkin exhibit large oscillations. Up to this point, we have not found any advantage of DRD over SUPG, in fact DRD behaved very similarly to Galerkin. Consider now the case A_4 ($\mathrm{Pe} = -1$, $r = 10$; $u = -40$, $c = 4 \times 10^3$, see Fig. 17). The inviscid approximation continues to be valid and the downwind boundary layer is very small, but now the characteristic length for the inviscid solution is $|u|/c = 10^{-3} \ll \bar{h}$, so that the solution is not 'smooth', and SUPG exhibits oscillations

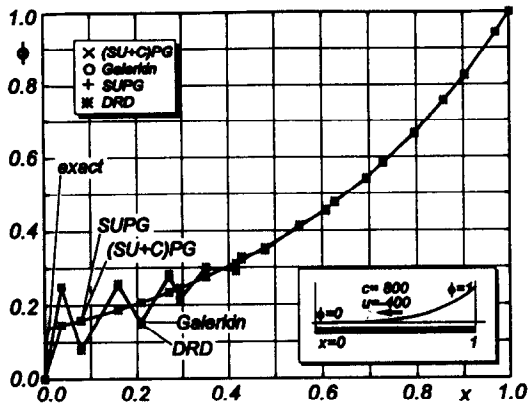

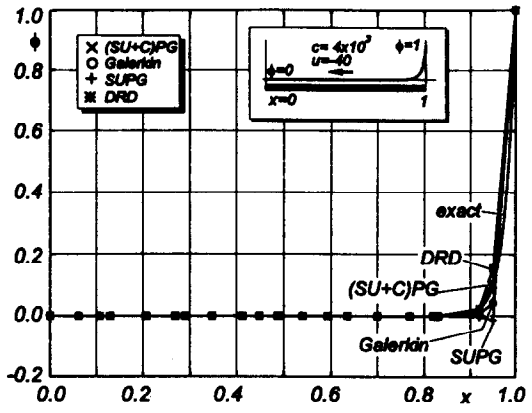

Fig. 16. One-dimensional example with non-uniform mesh. Case A_3.

Fig. 17. One-dimensional example with non-uniform mesh. Case A_4.

whereas DRD behaves very well. If we increase r to 50 ($c = 2 \times 10^4$) case A_5, see Fig. 18, the overshoot for SUPG is more pronounced, whereas DRD continues to be stable. This region, where $r \gg \|\mathrm{Pe}|$, and $\mathrm{Pe} < 0$ is the region where DRD signifies an improvement over SUPG. However, as was shown, DRD will fail whenever a diffusive boundary layer is expected. In contrast, *the* (SU + C)PG *method was stable uniformly over the whole* Pe-*r plane.*

6.3. *Sensitivity for unstructured meshes*

As the (SU + C)PG scheme was designed under uniform mesh conditions, it is interesting to see how it responds when the scale of the perturbation $\delta_{\max}$ is increased from 0 to 0.95. We used $N = 20$ ($\tilde{h} = 0.05$) and we performed the calculations for a problem with $u = 40$ (Pe = 1), $c = 4 \times 10^3$ ($r = 10$) with Dirichlet boundary conditions $\phi(0) = 0$, $\phi(1) = 1$ and no source term. The calculations were given for 20 values of $\delta_{\max}$ in the range $0 < \delta_{\max} < 0.95$, with 20 meshes for each value. In Fig. 19 we see a logarithmic plot of the maximum nodal error versus $\delta_{\max}$, where the maximum norm of the nodal error for a given mesh M is computed as

$$e_{\mathrm{nod,max}}(M) = \max_{j=0}^{N} |\phi_j - \phi_{\mathrm{ex},j}| , \tag{43}$$

where $\phi_{\mathrm{ex},j} = \phi_{\mathrm{ex}}(x_j)$ are the nodal values of the exact solution ϕ_{ex}. We are interested in the upper

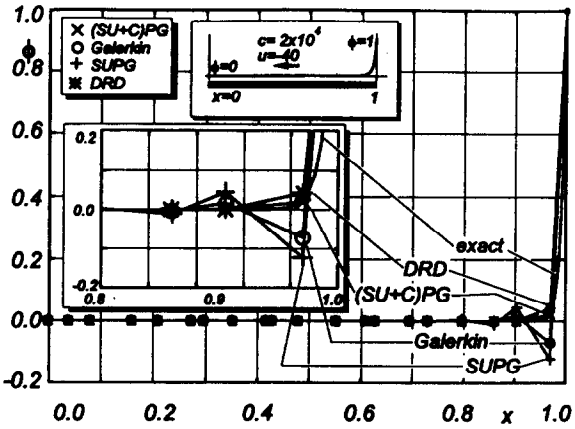

Fig. 18. One-dimensional example with non-uniform mesh. Case A_5.

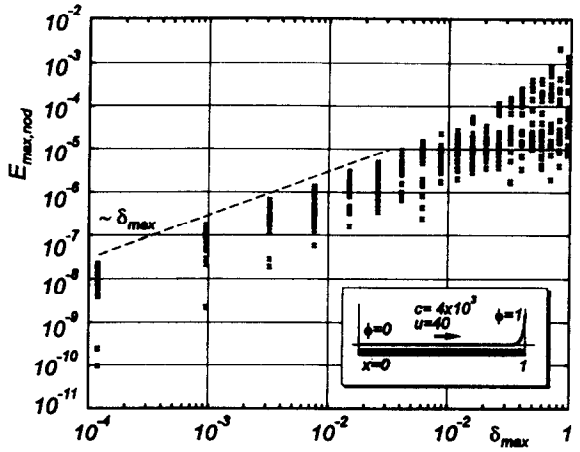

Fig. 19. Maximum nodal error over randomly generated non-uniform meshes as a function of the scale of the random perturbation.

envelope of the cloud of points, i.e. to the maximum error over all the meshes generated by a given $\delta_{\max}$:

$$E_{\text{nod,max}}(\delta_{\max}) = \max_{M \in \mathcal{M}} e_{\text{nod,max}}(M) . \tag{44}$$

Firstly, note that as $\delta_{\max} \to 0$, the upper envelope of the error also vanishes, apparently with an order $\delta_{\max}$. This is the *super-convergence limit*. On the other limit, as $\delta_{\max} \sim 1$ the error increases to values in the expected range.

6.4. Rate of convergence in non-uniform meshes

The next step is to assess the rate of convergence as the mesh is refined when the scheme is used in non-uniform mesh conditions. To do this, $\delta_{\max}$ is set to 0.8, and N takes the values 20, 50, 100, 200. 20 meshes are used for each value of N. In Fig. 20 we can see a logarithmic plot of the error versus $\bar{h}$, when the physical properties are such that Pe = 20, $r = 400$, whereas Fig. 21 corresponds to Pe = 20, $r = 4000$. It is observed that the upper envelope $E_{\text{nod,max}}(\bar{h})$ has a convergence order $\sim h^{4.48}$. Although this is a more realistic rate of convergence, it is far more optimistic than the optimal rates of convergence for the usual norms. This is due to the fact that we are using the nodal error.

6.5. Non-constant physical properties

In this example, the physical properties u and c are not constant over the domain and non-uniform meshes are used:

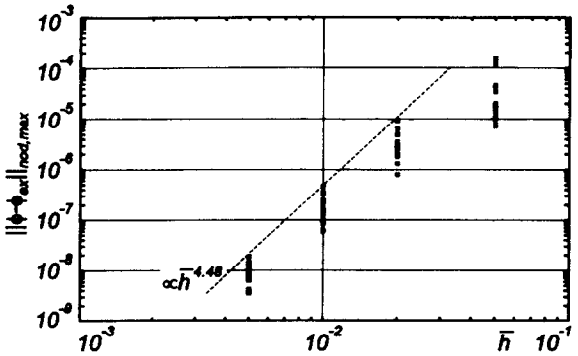

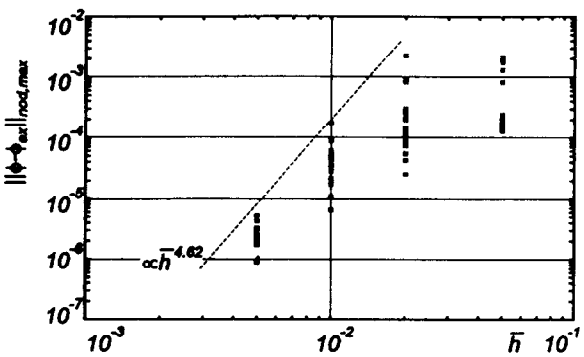

Fig. 20. Experimental determination of the rate of convergence for the maximum nodal error on non-uniform meshes.

Fig. 21. Experimental determination of the rate of convergence for the maximum nodal error on non-uniform meshes.

$$
\begin{aligned}
&N = 20\,,\\
&k = 1\,,\\
&\delta_{\max} = 0.8\,,\\
&u = \begin{cases} u_1 = -1\,; & x < 0.5\,;\\ u_2 = -10\,; & x < 0.5\,; \end{cases}\\
&c = \begin{cases} c_1 = 4\times 10^3\,; & x < 0.5\,;\\ c_2 = 1\,; & x < 0.5\,. \end{cases}
\end{aligned}
\tag{45}
$$

The exact solution is found by putting

$$
\phi(x) = \begin{cases} \phi_1(x) = A\exp\{\lambda_1 x\} + B\exp\{\lambda_2 x\}\,, & \text{for } x \leqslant \tfrac{1}{2}\,,\\ \phi_2(x) = C\exp\{\lambda_3 x\} + D\exp\{\lambda_4 x\}\,, & \text{for } x \geqslant \tfrac{1}{2}\,, \end{cases}
\tag{45}
$$

where λ_j are the solutions of the characteristic equations in both regions:

$$
\begin{aligned}
&\lambda_{1,2} = u_1/k \pm \sqrt{(u_1/k)^2 + c_1/k}\,,\\
&\lambda_{3,4} = u_2/k \pm \sqrt{(u_2/k)^2 + c_2/k}\,,
\end{aligned}
\tag{46}
$$

and A, B, C and D are constants that are adjusted in order to satisfy the boundary conditions at $x = 0$ and 1 and the matching conditions at $x = \frac{1}{2}$:

$$
\begin{aligned}
&\phi_1(0) = 0\,,\\
&\phi_2(1) = 1\,,\\
&\phi_1(x = \tfrac{1}{2}) = \phi_2(x = \tfrac{1}{2})\,,\\
&k\frac{\partial \phi_1}{\partial x}\bigg|_{x=\frac{1}{2}^-} = k\frac{\partial \phi_2}{\partial x}\bigg|_{x=\frac{1}{2}^+}\,.
\end{aligned}
\tag{47}
$$

The numerical solution is shown in Fig. 22, along with the Galerkin solution and the exact one. While the solution in the $x \geqslant \frac{1}{2}$ region is smooth, the solution in $x \leqslant \frac{1}{2}$ has a transition zone with a scale length 0.015, that is smaller than the average element size $\bar{h} = 0.05$. Consequently, Galerkin's method suffers from oscillations whereas the (SU + C)PG one remains stable.

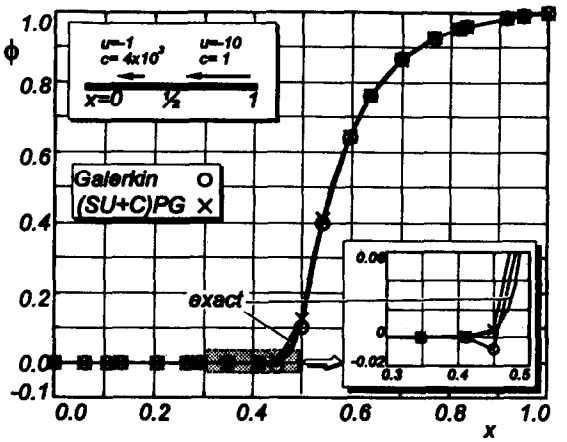

Fig. 22. Example with non-constant physical properties. Comparison between the different methods.

6.6. Example with internal source and null advection

Here, a source term along with non-uniform meshes are used. The physical constants, source term and boundary conditions are

$$\begin{aligned} &N = 20\,,\\ &k = 1\,,\\ &u = 0\,,\\ &c = 8\times 10^3\,,\\ &\delta_{\max} = 0.8\,,\\ &f(x) = \begin{cases} 0\,, & \text{if } x < \tfrac{1}{2}\,;\\ c\,, & \text{if } x > \tfrac{1}{2}\,;\end{cases}\\ &\phi(0) = \phi_0 = 0\,,\\ &\phi(1) = \phi_1 = 1\,. \end{aligned} \tag{48}$$

The exact solution is given by

$$\phi_{\mathrm{ex}}(x) = \begin{cases} \tfrac{1}{2}\sinh(\lambda x)/\sinh(\lambda/2)\,; & \text{for } x \leqslant \tfrac{1}{2}\,,\\ 1 - \tfrac{1}{2}\sinh[\lambda(1-x)]/\sinh(\lambda/2)\,; & \text{for } x \geqslant \tfrac{1}{2}\,, \end{cases} \tag{49}$$

where $\lambda = \sqrt{c/k} \approx 89.4$. Note that the resolution possesses reflection symmetry about $x = \frac{1}{2}$, $\phi = \frac{1}{2}$: $\phi(1-x) = 1 - \phi(x)$. The solution ϕ is S-shaped and for $c \to \infty$ it approaches a step function about $x = \frac{1}{2}$. The scale of the transition zone from $\phi = 0$ to $\phi = 1$ is $O(\sqrt{k/c})$. For large c, this discontinuity induces oscillations for the non-stabilized algorithms, so that it is a good test in order to show the benefits of the (SU + C)PG scheme. The numerical results are shown in Fig. 23, comparing the solution with the present method and Galerkin. For the given physical data, the scale of the transition zone from $\phi = 0$ to $\phi = 1$ is $\sim\sqrt{k/c} = 0.011$, being smaller than the average element size $\bar{h} = 0.05$. Therefore, Galerkin method produces spurious oscillations, whereas the (SU + C)PG method does not.

We have also performed a number of numerical tests to assess the rate of convergence with mesh refinement for this particular problem. We have performed the numerical computations on a family of 20 non-uniform meshes generated as explained previously, for $N = 20$, 50, 100 and 200 (see Fig. 24). The numerical parameters k, u, c, $\delta_{\max}$ and the boundary conditions are the same as before. We see that

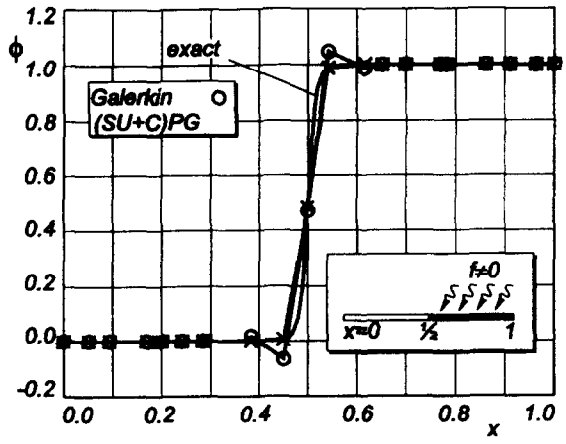

Fig. 23. Example with internal source and null advection. Comparison between the different methods.

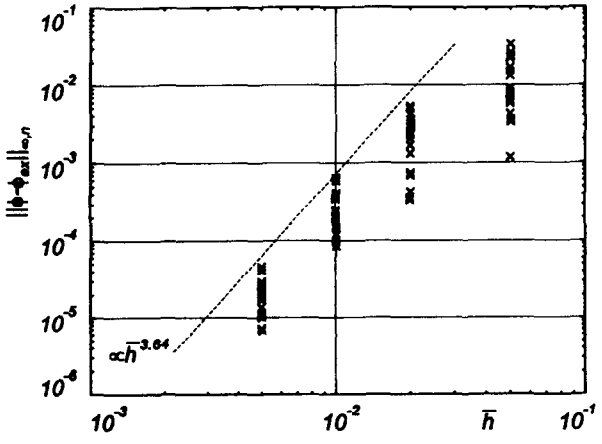

Fig. 24. Example with internal source and null advection. Convergence of maximum nodal error as a function of average mesh size.

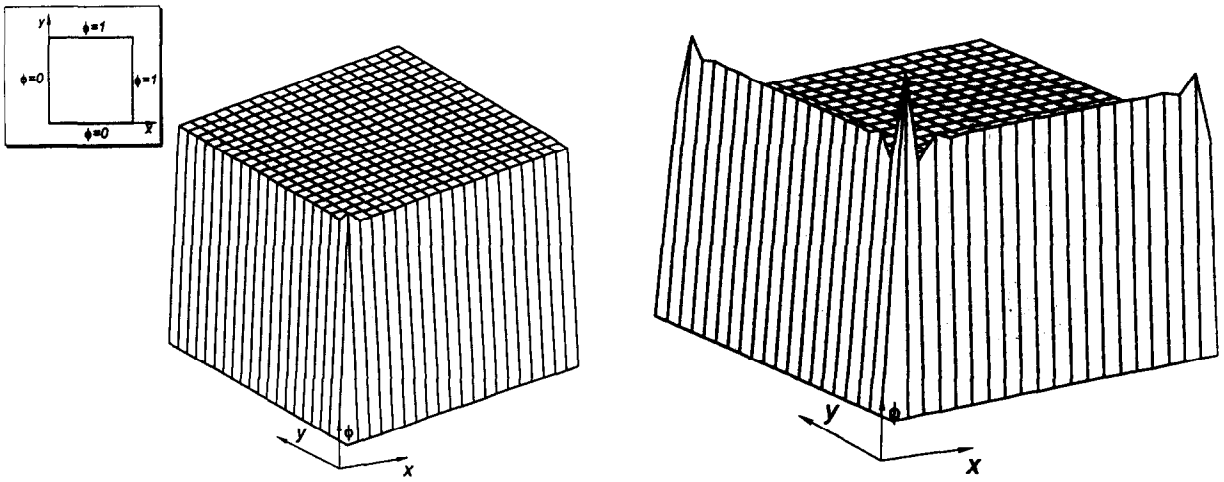

Fig. 25. Two-dimensional example. Null advection, $r_h = 2.5 \times 10^5$. Stabilized scheme.

Fig. 26. Two-dimensional example. Null advection, $r_h = 2.5 \times 10^5$. Galerkin.

the maximum nodal error over the set of meshes generated for a given N (and then of $\bar{h}$) and $\delta_{\max}$ behaves like: $E_{\text{nod,max}}(\bar{h}) \sim \bar{h}^{3.64}$.

6.7. *Multi-dimensional results*

The third test corresponds to a two dimensional example [4]. The uniform mesh is defined by 20×20 elements with a constant source term $f = 1$, null advection and $c = 1$, $k = 10^{-8}$, so that the element reaction number is equal to $r = 2.5 \times 10^5$. The boundary conditions are the following:

$$\phi(0, y) = \phi(x, 0) = 1 \quad \text{for } 0 \leqslant x,\ y \leqslant 1\,,$$
$$\phi(1, y) = \phi(x, 1) = 0 \quad \text{for } 0 \leqslant x,\ y \leqslant 1\,.$$

Figs. 25 and 26 show the numerical results with the stabilized scheme and with the Galerkin scheme. The numerical oscillations disappear with the present method as in previous one-dimensional problems.

Finally we performed another two-dimensional example that consists of a linear convection reaction without source term but, now, the velocity is not constant [4]. The domain is the unit square $0 \leqslant x, y \leqslant 1$. The velocity $\boldsymbol{u} = (u, v)$ is assumed to have a parabolic profile:

$$u(y) = u_{\max} y^2\,, \qquad v \equiv 0\,.$$

The reaction coefficient is equal to $c = 5$, diffusivity $k = 10^{-8}$ and $u_{\max} = 1$. The mesh is uniform and consists of 20×20 elements. The boundary conditions are natural (null flux) in three of the four sides of the domain and in the fourth side we have imposed a Dirichlet condition fixing the solution value equal to 1, as shown in Fig. 27. Figs. 27 and 28 show the stabilized scheme results and the standard SUPG ones. We can observe that the oscillations obtained with the standard SUPG near the zone where a very high reaction number exists have disappeared with the stabilized scheme whereas, in the rest of the domain, both solutions are equivalent since the problem is advection-dominated there.

7. Conclusions

This paper presents a stabilized multidimensional scheme for advection–reaction–diffusion problems that extends the SUPG method to overcome the numerical oscillations that appear from the reaction term. This numerical improvement allows us to treat, in an optimal way, a lot of industrial interesting situations where reaction effects are important in some regions of the domain, advection effects dominate in other zones, specially if the location of these zones is a priori unknown. It has been shown

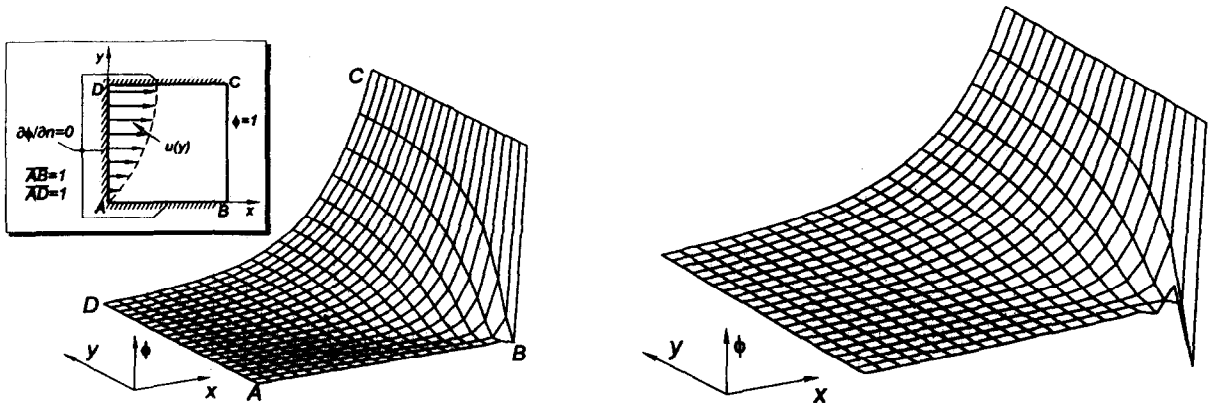

Fig. 27. Two-dimensional example with advection (parabolic profile). $c = 5$, $u_{max} = 1$, $k = 10^{-8}$. Problem description and numerical results with the (SU + C)PG scheme.

Fig. 28. Two-dimensional example with advection (parabolic profile). $c = 5$, $u_{max} = 1$, $k = 10^{-8}$. SUPG scheme.

that (SU + C)PG scheme satisfies the DMP criterion uniformly over all the Pe-r plane and it has been proved stable also in a series of numerical tests.

Acknowledgment

The authors wish to express their gratitude to Consejo Nacional de Investigaciones Científicas y Técnicas (CONICET, Argentina) for its financial support.

References

[1] A. Brooks and T.J.R. Hughes, Streamline upwind Petrov–Galerkin formulations for convection dominated flows with particular emphasis on the incompressible Navier–Stokes equations, Comput. Methods Appl. Mech. Engrg. 32 (1982) 199–259.

[2] T.J.R. Hughes and M. Mallet, A new finite element method for CFD: IV. A discontinuity-capturing operator for multidimensional advective–diffusive systems, Comput. Methods Appl. Mech. Engrg. 58 (1986) 329–336.

[3] T. Tezduyar and Y. Park, Discontinuity capturing finite element formulations for nonlinear convection–diffusion–reaction equations, Comput. Methods Appl. Mech. Engrg. 59 (1986) 307–325.

[4] R. Codina, A shock capturing anisotropic diffusion for the finite element solution of the diffusion–convection–reaction equation, in: E. Oñate, ed., Numerical Methods in Engineering and Applied Sciences (CIMNE, Barcelona, Spain, 1993).

[5] T.J.R. Hughes, L. Franca and M. Balestra, A new finite element formulation for CFD: V. Circumventing the Babuska–Brezzi condition: A stable Petrov–Galerkin formulation of the Stokes problem accommodating equal-order interpolations, Comput. Methods Appl. Mech. Engrg. 59 (1986) 85–99.

[6] T.J.R. Hughes, L. Franca and M. Mallett, A new finite element formulation for CFD: VI. Convergence analysis of the generalized SUPG formulation for linear time-dependent multidimensional advective–diffusive systems, Comput. Methods Appl. Mech. Engrg. 63 (1987) 97–112.

[7] L. Franca and E. Dutra do Carmo, The Galerkin gradient least-squares method, Comput. Methods Appl. Mech. Engrg. (1989) 41–54.

[8] M. Storti, N. Nigro and S. Idelsohn, A Petrov–Galerkin formulation for the advection–reaction–diffusion equation, Rev. Int. Mét. Núm. para Cálc. Dis. Ing. 11 (1995) 247–270.

[9] P.G. Ciarlet and P.A. Raviart, Maximum principle and uniform convergence for the finite element method. Comput. Methods Appl. Mech. Engrg. 2 (1973) 17–31.